Adsorption (2013) 19:967–977
DOI 10.1007/s10450-013-9508-5

# Carbon dioxide sequestration and methane removal from exhaust gases using resorcinol–formaldehyde activated carbon xerogel

**Ahmed Awadallah-F · Shaheen A. Al-Muhtaseb**

Received: 25 June 2012 / Accepted: 5 February 2013 / Published online: 20 February 2013


**Abstract** The world is faced with intrinsic environmental issues. Among these issues, the minimization of greenhouse gas emission to acceptable levels presents a high priority. This study seeks to help to reduce the greenhouse effect in sustainable manner. A resorcinol–formaldehyde xerogel was synthesized at specific conditions and used to prepare an activated carbon xerogel (RF-ACX). RF-ACX exhibited micropores in range of 1.2–1.4 nm, a surface area of 496 $m^2/g$ and a cumulative pore volume of 0.81 $cm^3/g$. Scanning electron microscopy showed that it is made of microspherical particles with an almost uniform particle size of 1.3 ± 0.2 μm. Equilibrium and kinetic studies for the adsorption of $CO_2$, $CH_4$ and $N_2$ on RF-ACX were conducted at five temperatures (293, 303, 313, 323, and 333 K) and pressures of up to 1 MPa. The adsorption capacity on RF-ACX was highest for $CO_2$, followed by $CH_4$ and then $N_2$. Isosteric heats of adsorption and adsorption rates were investigated. The measured adsorption equilibria were fitted with the extended multisite Langmuir adsorption model and further used to predict adsorption equilibria of their corresponding binary systems.

**Keywords** Resorcinol formaldehyde · Activated carbon · Xerogel · Adsorption · Greenhouse gases

**Electronic supplementary material** The online version of this article (doi:10.1007/s10450-013-9508-5) contains supplementary material, which is available to authorized users.

Ahmed Awadalla-F is on leave from the National Center for Radiation Research and Technology, P.O. Box 29, Nasr City, Cairo, Egypt.

A. Awadallah-F · S. A. Al-Muhtaseb (✉)
Department of Chemical Engineering, Qatar University, P.O. Box 2713, Doha, Qatar
e-mail: s.almuhtaseb@qu.edu.qa

## 1 Introduction

The world's high demand of fossil fuels led to escalating environmental concerns related to the healthy air quality and the recovery of greenhouse gases. As a result, an increasing attention is given to the removal and recovery of pollutants from gas mixtures, such as sour natural gas streams or exhaust gases produced from combustion processes. The generation and discharge of carbon dioxide into the atmosphere due to the consumption of large quantities of fossil fuels has emerged as a significant pollution problem for the environment (Liu et al. 2011). Effective $CO_2$ sequestration processes are essential to be developed. Industrial exhaust gas emissions contain mainly $CO_2$ and $N_2$ with traces of volatile organic compounds such as methane. As a result, the separation of $CO_2$, $N_2$ and $CH_4$ mixtures is very important for economic and environmental reasons. Methane is a potent greenhouse gas, which is estimated to have a 20-year global warming potential, 35 times which of carbon dioxide at equivalent emission rates (Long et al. 2010), so it must be reduced before emitted into the atmosphere (Zhang et al. 2009).

Recently, because of the sharp increase in oil prices and stringent environmental regulations, a significant increase has been witnessed in the production of natural gas as an efficient and environmentally clean fuel supply (Washington Policy and Analysis Inc. 2000). Unfortunately, the presence of contaminating gases such as carbon dioxide, hydrogen sulfide and nitrogen hinders the efficient utilization of natural gas. For instance, the acidic nature of $CO_2$ can result in corroding the pipeline and/or storage system in the presence of water. Furthermore, in addition of having no heating value, the presence of $CO_2$ and $N_2$ in natural gas reduces its combustion efficiency. As a result, natural gas streams containing $N_2$ or $CO_2$ need to be upgraded to meet

the "pipeline quality" of methane ($CH_4$) where the maximum amount of $CO_2$ and $N_2$ cannot exceed 2 % (Yang 2003; Tagliabue et al. 2012) and 4 % (Yang 2003), respectively.

Adsorption is considered to be among the most effective separation processes for gas streams. Nonetheless, such effectiveness cannot be obtained unless an optimum adsorbent is chosen with discrete affinities, capacities or adsorption kinetics for the corresponding gas species. Microporous activated carbons are very promising for being used in numerous applications (such as adsorbents, catalyst supports, and capacitors) (Muleja et al. 2012), because of their unique pore structures, low cost, and abundance of their raw ingredients (Xia et al. 2007). Carbon materials prepared by polymerization of hydroxylated benzene and aldehydes in a solvent, followed by drying and pyrolysis have been extensively studied over the past decade (Al-Muhtaseb and Ritter 2003; Czakkel et al. 2012; Gallegos-Suarez et al. 2012). This route can result in various carbon materials whose textures depend on the nature of precursors, gelation conditions, drying method and carbonization and activation procedures (Czakkel et al. 2012; Gallegos-Suarez et al. 2012; Rasines et al. 2012). The most common precursors are resorcinol and formaldehyde; and the polymerization process is usually conducted in water as a solvent with $Na_2CO_3$ as a catalyst (Awadallah-F et al. 2011; ElKhatat and Al-Muhtaseb 2011). Resorcinol–formaldehyde (RF) materials are known for their wide range of characteristics resulting from various synthesis conditions. This makes them and their corresponding activated carbons suitable candidates for a wide range of applications. However, it is important to know how to create or tailor carbon materials with ease of handling, along with favorable pore properties for specialized practical uses. Recently, organic and carbon RF xerogels have received an increasing interest for their wide applicability as adsorbents due to their special pore properties (Morales-Torres et al. 2012).

In this paper, a potential pathway to help minimize greenhouse by adsorption is investigated. This leads to finding related to the carbon dioxide sequestration and methane removable potentials. Microporous RF activated carbon xerogels (RF-ACX) were prepared and characterized. Then, they were utilized for the adsorption of $CO_2$, $CH_4$, and $N_2$ gases at wide ranges of temperatures and pressures. Adsorption experiments were conducted at different temperatures and pressures. The experimental data were analyzed using the extended multisite Langmuir's model. Also, the isosteric heats of adsorption were estimated from measured adsorption data, and were compared for various species at different adsorption conditions to explore the interactions between the adsorbent and adsorbate molecules. The overall mass transfer coefficients for the adsorption of $CO_2$, $CH_4$ and $N_2$ were also examined versus the corresponding values of pressures and temperatures to judge on the possibilities of kinetic adsorption separations of their mixtures.

## 2 Experimental

### 2.1 Materials

Resorcinol (ACS, 99.98 %, Alfa Aesar), formaldehyde (37 wt% in $H_2O$ with 10–15 % methanol as stabilizer, Aldrich), sodium carbonate (anhydrous, ACS, Fisher) and acetone (optima, 99.6 %, Fisher) were used as received. Ultra purified water produced from Milli-Q integral water purification system was used in the experiments. Other reagents ($CH_3COOH$, $HNO_3$ and $NH_4OH$) are analytical grade. All gases used in the experiments ($CO_2$, $CH_4$, $N_2$, He) were supplied by NIGP (Doha-Qatar) with grade-5 purity (>99.999 %).

### 2.2 Preparation of resorcinol–formaldehyde carbon xerogel

The preparation of RF xerogels has been described previously (Awadallah-F et al. 2011). Xerogels were prepared with molar ratios of resorcinol-to-formaldehyde of 0.5, resorcinol-to-water of 0.05, and resorcinol-to-catalyst of 500. Resorcinol (11.1252 g) and sodium carbonate (0.0214 g) were weighted and mixed with ultrapure water (29.15 $cm^3$) in Erlenmeyer flasks and stirred magnetically for 3 h to guarantee that all resorcinol and sodium carbonate are completely dissolved. Then, formaldehyde (15.56 $cm^3$) was added to the dissolved ingredients. After that, the solution acidity was adjusted to a pH of 7.0 ± 0.1 by using diluted $HNO_3$ and $NH_4OH$. RF solutions were then poured into cylindrical polypropylene vials, sealed and placed in an oven at 343 K for 7 days to complete their curing. In order to prevent the dehydration of the gels, and to accelerate gelation time and enhance their cross-linking, 2 % $CH_3COOH$ was poured upon the gels surfaces after partial solidification. Further experimental details are given elsewhere (Awadallah-F et al. 2011). Subsequently, RF xerogels were carbonized, activated and characterized as explained in the Online Resource Sections S1 and S2, respectively.

## 3 Theory

### 3.1 Adsorption equilibrium

The extended multisite Langmuir model assumes that the energetically heterogeneous adsorbent surface is composed of a number of patches with distinct adsorption energies. Each patch is thus considered as a homogeneous portion of

the adsorbent surface; and the total amount adsorbed of a pure gas can be expressed as:

$$n_{\text{ads}} = \sum_{j=1}^{J} \frac{m_j b_j P}{1 + b_j P} \quad (1)$$

where $J$ is the number of homogeneous adsorption patches (usually set to 2 or 3, depending on the extent of heterogeneity), $j$ the adsorption patch number, $P$ is pressure, $m_j$ is monolayer adsorption capacity of the adsorbed component on the $j$th adsorption patch; and $b_j$ is the adsorption affinity on patch $j$ which is given by:

$$b_j = b_j^0 \exp\left(\frac{\varepsilon_j}{RT}\right) \quad (2)$$

where $b_j^0$ is the adsorption affinity on patch $j$ at infinite temperature and $\varepsilon_j$ is the characteristic adsorption energy on patch $j$, $R$ is the universal gas constant and $T$ is absolute temperature.

This model can be used confidently to predict binary and multicomponent adsorption equilibria (Ritter et al. 2011), where the amount adsorbed of component $i$ in a mixture containing $N$ components can be predicted using the following equation

$$n_i = \sum_{j=1}^{J} \frac{m_{i,j} b_{i,j} P}{1 + \sum_{k=1}^{N} b_{k,j} y_k P} \quad (3)$$

where $j$ is a counter for homogeneous adsorption sites (or patches) and $k$ is a counter for components. The mole fractions $y_i$ and $y_k$ are, respectively, for components $i$ and $k$ in the gas phase.Upon calculating the amount adsorbed of each component in the mixture, the mole fraction of each component ($i$) in the adsorbed phase can be calculated from

$$x_i = \frac{n_i}{\sum_{k=1}^{N} n_k} \quad (4)$$

where $n_i$ and $n_k$ are the amounts adsorbed of components $i$ and $k$, respectively. Accordingly, the adsorbent's selectivity to adsorb component "$i$" relative to component "$k$" ($S_{i,k}$) in a binary mixture is given by

$$S_{i,k} = \frac{\left(\frac{x_i}{y_i}\right)}{\left(\frac{x_k}{y_k}\right)} \quad (5)$$

where $x$ and $y$ are the mole fractions of the corresponding component ($i$ or $j$) in the adsorbed and gas phases, respectively.

### 3.2 Isosteric heat of adsorption

The isosteric heat of adsorption ($-\Delta Q_{\text{st}}$), can be evaluated from experimental nonisothermal adsorption data by Clausius-Clapeyron equation as (Rahman et al. 2012),

$$\Delta Q_{\text{st}} = -R \left[\frac{\partial \ln P}{\partial (1/T)}\right]_n \quad (6)$$

The variation of isosteric heat of adsorption with surface coverage is an indirect measure of the interactions among adsorbate molecules and between adsorbate molecules and adsorbent lattice atoms. It also indicates the energetic heterogeneity of a solid surface.

### 3.3 Adsorption kinetics

The rate of adsorption can be determined through the linear driving force (LDF) model (Al-Muhtaseb and Ritter 1999), which gives

$$\frac{m_t}{m_e} = 1 - e^{-kt} \quad (7)$$

where $m_t$ the amount adsorbed at time $t$, $m_e$ is the equilibrium quantity adsorbed at the corresponding temperature and pressure; and $k$ is the overall mass transfer coefficient.

## 4 Results and discussion

### 4.1 Textural structure

Table 1 summarizes the pore characteristics obtained from surface area and porosity analyzer, with various structural characteristics summarized in Fig. 1. Figure 1a shows the adsorption/desorption isotherm for nitrogen at 77 K onto RF-ACX. This behavior corresponds mostly to Type I adsorption isotherm, and has a well-defined plateau according to the IUPAC classification which shows that all micropores are filled with nitrogen molecules and that no other pore types exist (thus, the pore width scales in Fig. 1b and c were truncated at 1.8 nm as no significant pores were indicated afterwards. Capillary condensation started at relative pressure >0.901 as indicated by the corresponding steep increase of uptake. The isotherm also shows a reversible desorption process where the adsorption and desorption curves coincide with each other. The maximum capacity of RF-ACX to adsorb $N_2$ at 77 K was 12 mol/kg.

**Table 1** Overall porous characteristics of RF-ACX obtained from the adsorption of $N_2$ at 77 K

| | |
|---|---|
| Total area from DFT method | 496 $m^2/g$ |
| Total micropore surface area derived from DFT | 494 $m^2/g$ |
| Total pore volume derived from DFT method | 0.37 $cm^3/g$ |
| Total micropore pore volume derived from DFT method | 0.31 $cm^3/g$ |
| Average micropore width | 1.51 nm |
| $N_2$ adsorption capacity at 77 K | 12.20 mol/kg |

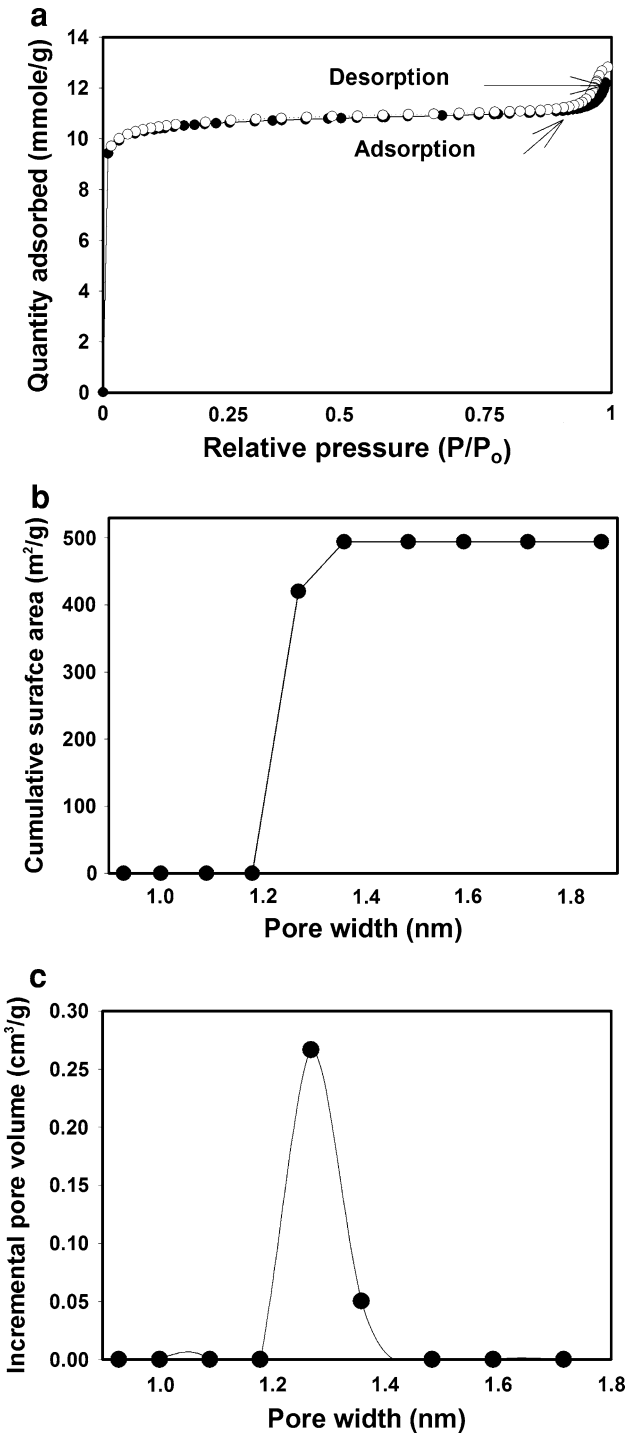


**Fig. 1** Textural structure analysis of RF-ACX: **a** $N_2$ adsorption–desorption isotherms at 77 K; **b** cumulative surface area distribution; and **c** incremental pore volume versus pore width

Figure 1b shows the cumulative surface area with pore sizes in the range from 0 to 1.9 nm. The cumulative surface area was nil within the pore width range between 0.8 and 1.2 nm, followed by sharp increase up to 496 $m^2/g$, which then remains almost constant at pore widths $> \sim 1.3$ nm.

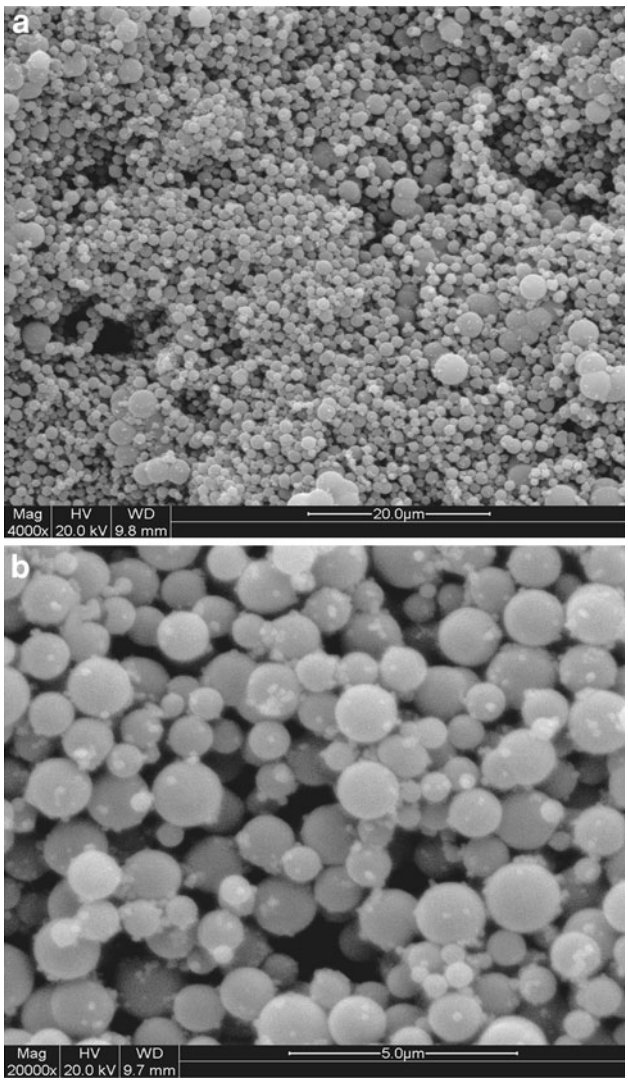


**Fig. 2** SEM photos of RF-ACX at different zoom levels; **a** scale bars of 20.0 and **b** 5.0 µm, respectively

This indicates that the whole surface area corresponds only to pore widths ranging from $\sim 1.2$ to 1.4 nm. Further, no significant portions of pores exist before 1.2 nm. This indicates that the accumulative surface area resembles a microheterogeneous regions, which exhibits a slightly spread distribution of micropores. This conclusion is also supported by the incremental pore volume distribution versus pore width (illustrated in Fig. 1c), where the majority of pore volume falls within the pore width range from $\sim 1.2$ to 1.4 nm.

Figure 2a, b show the SEM morphology of the microporous RF-ACX xerogel with magnifications of 4,000× and 20,000×, respectively. These photos show well-defined spherical particles. An average particle size of $\sim 1.3 \pm 0.2$ µm was observed.

### 4.2 Adsorption isotherms

Adsorption isotherms of $CO_2$, $CH_4$, and $N_2$ on RF-ACX were measured at pressures up to $\sim$1 MPa, and at different temperatures. A buoyancy correction was applied to the amounts adsorbed (Online Resource Section S3), and the corresponding absolute) amounts adsorbed of $CO_2$, $CH_4$, and $N_2$ are represented by symbols in Fig. 3. All the adsorption/desorption isotherms presented in Fig. 3 are of Type I of IUPAC classification, indicating the adsorption of molecules onto a dominantly microporous surface. This confirms the results deduced from Fig. 1a). The adsorbed amounts were highest for $CO_2$, intermediate for $CH_4$, and lowest for $N_2$. Such distinct adsorption capacities of these components on RF-ACX are highly advantageous for their separation. The adsorption of $CO_2$ and $CH_4$ approach saturation at the maximum pressure of $\sim$1 MPa as indicated in Fig. 3a, b. On the other hand, Fig. 3c shows that the adsorption of $N_2$ continues to increase almost linearly with pressure. Thus, it is anticipated for $N_2$ to reach the saturation at higher pressures.

### 4.3 Fitting adsorption data

The measured absolute adsorption/desorption for $CO_2$, $CH_4$, and $N_2$ onto the RF-ACX are fitted using the multisite Langmuir model by finding the optimum set of $3\times J$ fitting parameters ($m_j$, $b_j^0$ and $\varepsilon_j$ for each homogeneous patch, $j$, of the total number of $J$ patches) that yield the least sum of squared errors (LSSE), which is defined as:

$$\text{LSSE} = \text{minimum}\left\{\sum_{i}^{N_P}\left(n_{\text{cal}} - n_{\text{exp}}\right)_i^2\right\} \tag{8}$$

where $i$ is data point number, $N_P$ is the total number of data points for each component and the subscripts "exp" and "cal" denote, respectively, experimental and calculated amounts, with the calculated amount obtained from Eqs. (1, 2). The optimum fitting parameters were obtained from the collective adsorption data at all temperatures as listed in Table 2 along with the corresponding percentage average relative error (ARE) for each component, which is defined by:

$$\text{ARE}\,(\%) = \frac{100\%}{N_P}\sum_{i}^{N_P}\left|\frac{n_{\text{cal}} - n_{\text{exp}}}{n_{\text{exp}}}\right|_i \tag{9}$$

The corresponding correlations are also depicted in Fig. 3 (lines) in comparison to the experimental data (symbols). It can be seen from Fig. 3 that the experimental data are well correlated with the Langmuir model for all components in spite of little deviations at very low pressures. Trials confirmed that only two homogenous patches

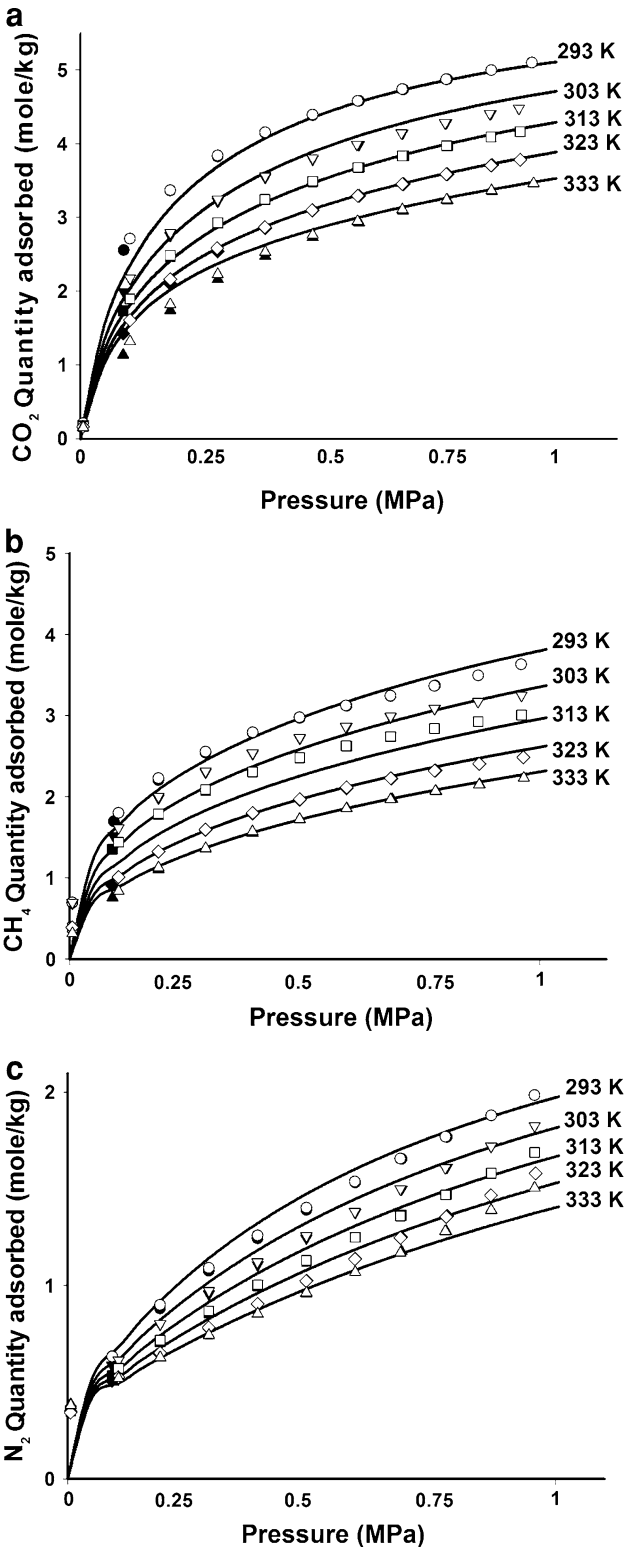


**Fig. 3** Experimental (*symbols*) and correlated (*lines*) adsorption equilibrium data using the extended multisite Langmuir adsorption model versus absolute quantity adsorbed of: **a** $CO_2$, **b** $CH_4$ and **c** $N_2$ onto RF-ACX at different temperatures. *Solid* and *empty symbol* denote, respectively, adsorption and desorption data

**Table 2** Optimum fitting parameters and ARE values of the extended multisite langmuir model for the absolute quantity adsorbed of $CO_2$, $CH_4$ and $N_2$ on RF-ACX at 20–60 °C

| Component | $j$ | $m_j$ (mol/kg) | $b_j^0$ ($MPa^{-1}$) | $E/R$ (K) | ARE (%) |
|---|---|---|---|---|---|
| $CH_4$ | 1 | 3.351 | $3.644 \times 10^{-6}$ | 4,140.719 | 3.976 |
| | 2 | 0.706 | $9.052 \times 10^{-4}$ | 3,944.738 | |
| $CO_2$ | 1 | 3.750 | $3.970 \times 10^{-4}$ | 3,108.469 | 4.145 |
| | 2 | 3.513 | $1.500 \times 10^{-7}$ | 4,558.720 | |
| $N_2$ | 1 | 4.155 | $3.081 \times 10^{-3}$ | 1,573.628 | 1.843 |
| | 2 | 0.375 | 886.521 | 318.268 | |

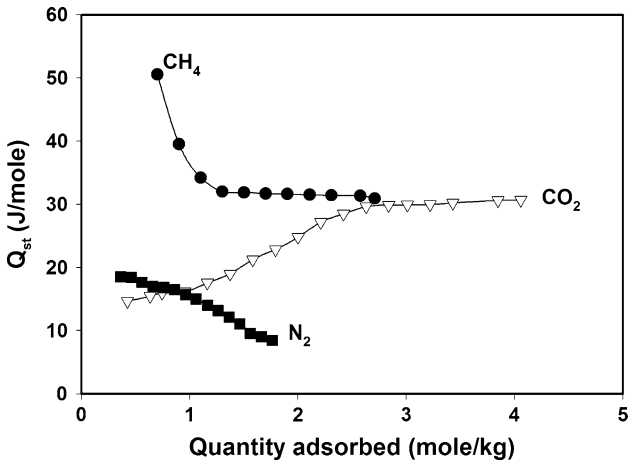


**Fig. 4** Effect of the quantity adsorbed on the isosteric heat of adsorption of $CH_4$, $CO_2$ and $N_2$ onto RF-ACX

($J = 2$) are sufficient to describe the adsorption of $CO_2$, $CH_4$ or $N_2$ via the multisite Langmuir adsorption model, which corresponds to the dual site Langmuir (Ritter et al. 2011).

### 4.4 Isosteric heat of adsorption

The isosteric heat of adsorption is an important indicator about adsorption affinity. Adsorption isotherms of $CH_4$, $CO_2$ and $N_2$ on RF-ACX were measured at five different temperatures, as shown previously in Fig. 3. These data were used for calculating the isosteric heats of adsorption according to Eq. 6.

Figure 4 shows the estimated isosteric heats of adsorption for $CH_4$, $CO_2$ and $N_2$ on RF-ACX as a function of the amounts adsorbed. For small amounts adsorbed (e.g., at ~1 mol/kg), the highest isosteric heat was for $CH_4$ (~35 kJ/mol), whereas almost equal isosteric heats (~13–20 kJ/mol) are exhibited for $CO_2$ and $N_2$ at ~0.5 mol/kg. This indicates that RF-ACX with low surface coverage has a higher affinity to adsorb $CH_4$ than $CO_2$ or $N_2$. Nonetheless, the isosteric heat of $CH_4$ decreases slightly to ~30 kJ/mol at an amount adsorbed of ~1.3 mol/kg, and remains constant afterwards. In the case of $CO_2$ adsorption, the isosteric heat increases with increasing loading until reaching ~30 kJ/mol at 2.7 mol/kg, and also remains constant afterwards. This indicates that favorable interactions exist among adsorbed $CO_2$ molecules, which contribute to increasing the adsorption affinity of $CO_2$ at higher surface coverage. On the other hand, the isosteric heat of $N_2$ decreases largely with increasing amount adsorbed. When increasing an amount adsorbed of $N_2$ to ~1.9 mol/kg, its isosteric heat falls to ~8.5 kJ/mol.

### 4.5 Overall mass transfer coefficient

For freely moving gases, the physics of random molecular motion lead to higher mass transfer rates with increasing temperature or decreasing pressure. Nonetheless, an in adsorbed phase, the rate of mass transfer does not fully comply with such physics as it might be affected by other factors related to the adsorbent. From the variations of the measured absolute amounts adsorbed with time (explained in Online Resource Section S3), the mass transfer coefficients can be obtained from Eq. 7 as the negative slope of $\ln(1 - m_t/m_e)$ versus $t$.

Figures 5a–c show the effect of pressure on the mass transfer coefficients for $CO_2$, $CH_4$ and $N_2$; respectively, onto RF-ACX at different temperatures. Overall, it can be found that the adsorption mass transfer coefficients ($k$) for all species comply to anticipated trends for gases with different extents. Figure 5a shows that the effect of pressure is independent from the effect of temperature as indicated from the almost parallel curves at different temperatures. Overall, increasing pressure from ~0 to ~1 MPa results in decreasing $k_{CO_2}$ by $\sim 4.8 \times 10^{-3}$ $s^{-1}$ at all temperatures. Furthermore, especially at low to moderate pressures, $k_{CO_2}$ decreased noticeably with increasing pressures, regardless of temperature. Nonetheless, at relatively high pressures, $k_{CO_2}$ becomes almost independent of pressure.

Figure 5b shows the effects of pressure and temperature on $k_{CH_4}$. Similar trends of pressure and temperature dependences were observed with $k_{CH_4}$ as was for the case for $k_{CO_2}$. Nonetheless, at relatively low pressures, $k_{CH_4}$ is higher than $k_{CO_2}$. As a result, since the adsorption capacity of RF-ACX for $CO_2$ is higher than that of $CH_4$, the use of RF-ACX for separating $CO_2$ from $CH_4$ presents an interesting case where the adsorption and desorption step durations would be among the key factors of the corresponding process. In other words, RF-ACX will be more selective for $CH_4$ than $CO_2$ at short times and vice versa at long times (when equilibrium is approached).

Figure 5c shows that $k_{N_2}$ behaves as expected, where it increases with increasing temperature and decreases with

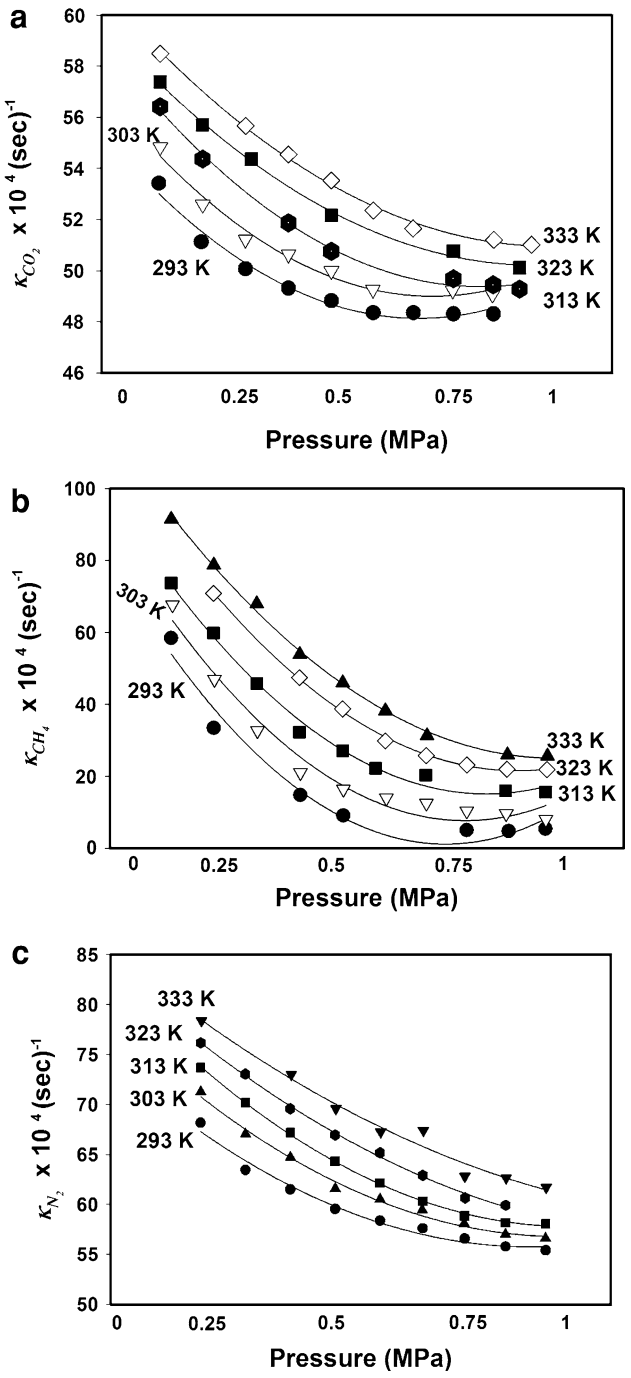


**Fig. 5** Estimated overall mass transfer coefficient for the adsorption of **a** $CO_2$, **b** $CH_4$ and **c** $N_2$ onto RF-ACX at different temperatures

increasing pressure in almost parallel straight lines. Nonetheless, like $CH_4$, at low pressures, the adsorption of $N_2$ is faster than that of $CO_2$; but comparable adsorption rates are exhibited at relatively high pressures. Oppositely, $k_{N_2}$ changes from being almost equivalent to $k_{CH_4}$ at low pressures to surpassing it at high pressures. This indicates that these components can be separated from each other by altering equilibrium and/or kinetic selectivities at different conditions. If long adsorption/desorption times are allowed in an adsorption process, then the equilibrium selectivity dominates the separation with an anticipated order of $CO_2 > CH_4 > N_2$. However, if short times are enforced where adsorption remains far from equilibrium, then the kinetic behavior dominates the process. In the latter case, the selectivity of RF-ACX is anticipated to follow the order of $CH_4 > N_2 > CO_2$ at low pressure or $N_2 \geq CO_2 > CH_4$ at high pressure.

### 4.6 Binary adsorption equilibria

The single component fitting parameters were used to predict the corresponding binary adsorption equilibria of $CO_2$ in $CH_4$ (which is of relevance to natural gas sweetening applications), $CH_4$ in $N_2$ (which is of relevance to the removal of hydrocarbons from exhaust gases) and $CO_4$ in $N_2$ (which is of relevance to the sequestration of carbon dioxide from off-gases). The effects of temperature and pressure were evaluated as a function of adsorbed phase mol fraction ($x$) in Figs. 6, 7 and 8. It has to be noted that these predictions do not consider the effects of adsorption kinetics which were discussed in the previous section because their effects fade if enough time is allowed for adsorption to reach equilibrium. If this is not the case (i.e., if the adsorption time is insufficient to reach equilibrium), then combined effects of adsorption kinetics and equilibrium have to be considered through rigorous adsorption process simulations which are not considered here.

Figure 6a shows the effect of adsorbed phase composition ($x_{CO_2}$) on gas phase composition ($y_{CO_2}$) at various temperatures and low and moderate pressures of 0.1 and 0.5 MPa, respectively. At low pressures, the system may exhibit an azeotropic behavior ($x_{CO_2} = y_{CO_2}$) at a wide range of temperature whereas the azeotropic composition decreases with increasing temperature. Nonetheless, when increasing the pressure to 0.5 MPa, the azeotropic composition shifts to around 80 % $CO_2$, and becomes almost unaffected with temperature. Figure 6b shows the variation of the adsorption selectivity with the $x_{CO_2}$. When adsorption is at low pressure (e.g., 0.1 MPa), the temperature effect becomes significant on both adsorption equilibria and the selectivity. At low pressure (resembled by 0.1 MPa), the selectivity of the adsorbent towards $CO_2$ ($S_{CO_2,CH_4}$) decreases with increasing temperature. At moderate $x_{CO_2}$, the adsorbent can change is selectivity from favoring $CO_2$ ($S_{CO_2,CH_4} > 1$) to favoring $CH_4$ ($S_{CO_2,CH_4} < 1$). Nonetheless, when increasing the pressure to 0.5 MPa, the adsorbent becomes more selective to $CO_2$ with a slight dependence on temperature up to $x_{CO_2} = \sim 0.75$, after which the adsorbent becomes more selective to $CH_4$. The slight dependence on temperature at high pressure is in agreement with the

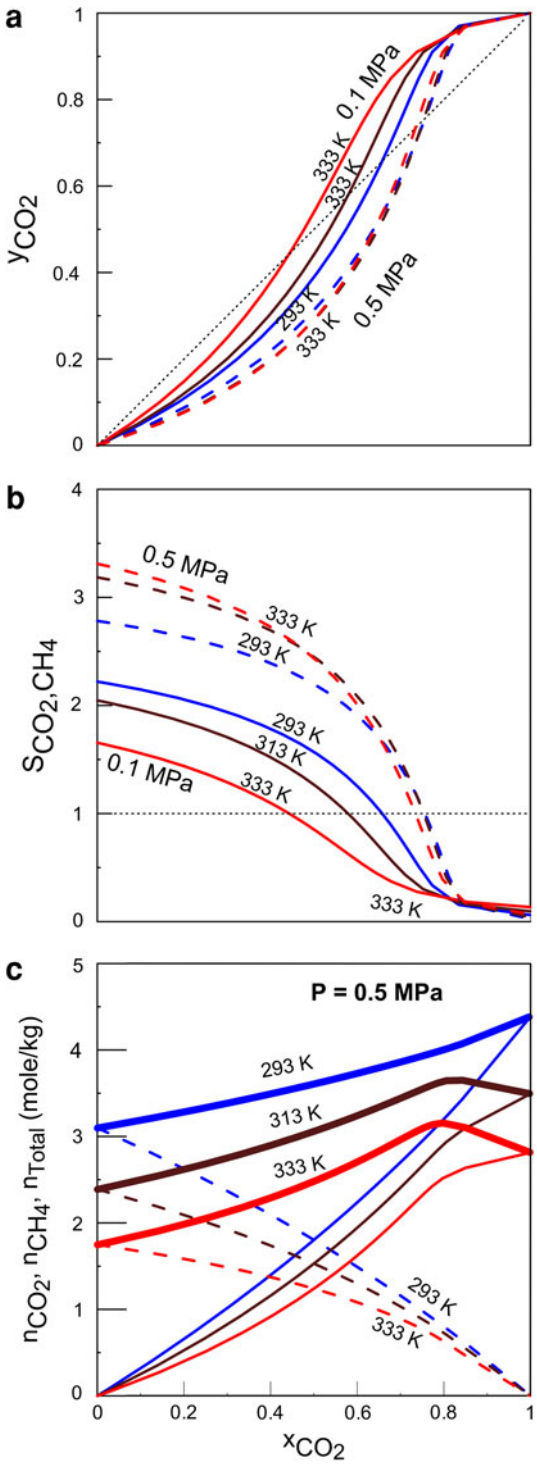


**Fig. 6** Predicted binary adsorption **a** equilibria and **b** selectivity of $CO_2$ and $CH_4$ at 0.1 and 0.5 MPa (*solid* and *dashed lines*, respectively) with *dotted lines* representing azeotropic behavior. Subfigure (**c**) shows the predicted binary amounts adsorbed of $CO_2$ (*thin solid lines*), $CH_4$ (*dashed lines*) and the total mixture (*thick solid lines*) at 0.5 MPa

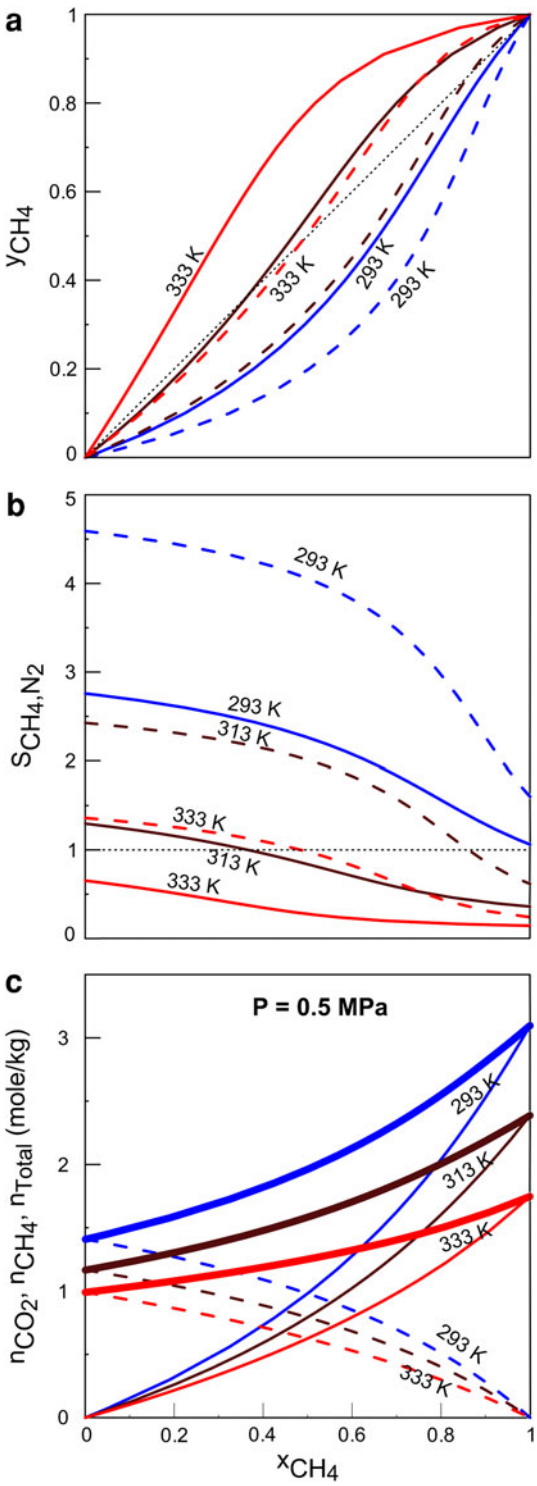


**Fig. 7** Predicted binary adsorption **a** equilibria and **b** selectivity of $CH_4$ and $N_2$ at 0.1 and 0.5 MPa (*solid* and *dashed lines*, respectively) with *dotted lines* representing azeotropic behavior. Subfigure (**c**) shows the predicted binary amounts adsorbed of $CH_4$ (*thin solid lines*), $N_2$ (*dashed lines*) and the total mixture (*thick solid lines*) at 0.5 MPa

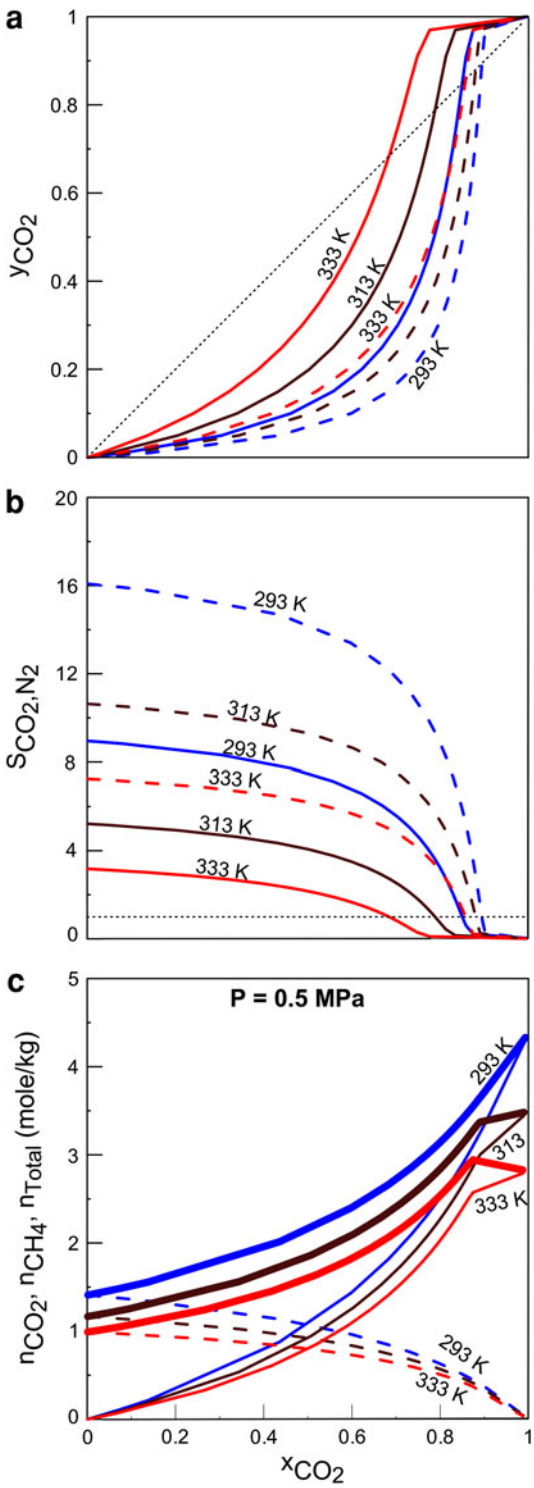


**Fig. 8** Predicted binary adsorption **a** equilibria and **b** selectivity of $CO_2$ and $N_2$ at 0.1 and 0.5 MPa (*solid* and *dashed lines*, respectively) with *dotted lines* representing azeotropic behavior. Subfigure (**c**) shows the predicted binary amounts adsorbed of $CO_2$ (*thin solid lines*), $N_2$ (*dashed lines*) and the total mixture (*thick solid lines*) at 0.5 MPa

isosteric heats of adsorption presented in Fig. 5 where both $CO_2$ and $CH_4$ exhibit almost equal values at high loading. It can be concluded that RF-ACX exhibits more distinct selectivities at high pressures where it provides better selectivity for $CO_2$ at low $x_{CO_2}$. The amounts adsorbed of $CO_2$, $CH_4$ and their mixture at an intermediate pressure are shown in Fig. 6c. In all cases, the total amount adsorbed decreases with increasing temperature and could exhibit a maximum amount corresponding at intermediate compositions where favorable interactions between the two components exist at temperatures of 313 K or above.

The effects of adsorbed phase composition, temperature and pressure on the gas phase composition and adsorption selectivity to $CH_4$ are shown in Fig. 7a and b, respectively. A maximum adsorption selectivity of $CH_4$ relative to $N_2$ ($S_{CH_4,N_2}$) is exhibited at high pressure (0.5 MPa) and low temperature (293 K), and no azeotropes are found at this condition. Nonetheless, the selectivity to $CH_4$ decreases with increasing temperature and with increasing $x_{CH_4}$. Adsorption azeotropes start to occur at high pressures if the temperature is high. At low pressure (i.e., at 0.1 MPa), $S_{CH_4,N_2}$ decreases significantly relative to that at 0.5 MPa. Nonetheless, like the former case, the selectivity towards $CH_4$ decreases with both increasing temperature and increasing $x_{CH_4}$. At temperatures higher than $\sim$333 K and low pressure, RF-ACX becomes more selective for $N_2$ than $CH_4$ at all compositions ($S_{CH_4,N_2} < 1$). The amounts adsorbed of $CH_4$, $N_2$ and their mixtures at an intermediate pressure are plotted in Fig. 7c. The amount adsorbed of the total mixture increases steadily when increasing $x_{CH_4}$ at all temperatures. Furthermore, the amounts adsorbed always decreased with increasing temperature.

The effects of pressure and temperature on the equilibrium compositions and selectivity of $CO_2$–$N_2$ mixtures is illustrated in Fig. 8. At most conditions, RF-ACX is more selective for $CO_2$ than $N_2$ ($S_{CO_2,N_2} > 1$), especially at high pressure, low temperature and low $CO_2$ concentration where $S_{CO_2,N_2}$ can reach as high as 16. Nonetheless, $S_{CO_2,N_2}$ decreases with decreasing pressure, increasing temperature or increasing $x_{CO_2}$. At high pressure (0.5 MPa), an azeotropic behavior is exhibited at $x_{CO_2} = \sim 0.90$, which is almost constant regardless of temperature. After this composition, RF-ACX becomes more selective for $N_2$ than $CO_2$ ($S_{CO_2,N_2} < 1$). At low pressure (0.1 MPa), $S_{CO_2,N_2}$ is significantly less than the case of higher pressure. Furthermore, azeotropic mixtures are exhibited for the low pressure case where the selectivity reversal is exhibited at $x_{CO_2}$ ranging from $\sim$0.68 at 333 to $\sim$0.85 at 293 K. As a result, an adsorbent which is mostly saturated with $CO_2$ can be regenerated easily by reducing pressure and increasing

temperature, which make it more selective for $N_2$ (lower $S_{CO_2,N_2}$). The predicted amounts adsorbed of $CO_2$, $N_2$ and their mixtures on RF-ACX at a moderate pressure are demonstrated in Fig. 8c. At high temperatures (313 K or above), maximum total amounts adsorbed are exhibited at $x_{CO_2}$ approximately corresponding to the azeotropic mixture compositions noted previously in Fig. 8a, b. This indicates that such compositions exhibit the highest favorable interactions among the adsorbed species and the adsorbent where the adsorption capacity of the adsorbent is maximized. Overall, the temperature effect was almost steady at all $x_{CO_2}$.

## 5 Conclusions

A resorcinol–formaldehyde activated carbon xerogel (RF-ACX) was synthesized at specific conditions. Pore structure characteristics and surface morphology of the RF-ACX were examined by surface area and porosity analyzer and scanning electron microscopy (SEM). The RF-ACX was found to exhibit a sharp pore size distribution ranging between 1.2 and 1.4 nm, which indicates a microporous structure. The surface morphology exhibited an almost homogeneous pattern of microspheres with an average size of $1.3 \pm 0.2$ μm.

The adsorption of pure gases ($CO_2$, $CH_4$ and $N_2$) on RF-ACX at various temperatures and pressures was investigated. Type-I reversible adsorption/desorption isotherms were exhibited, with different approaches towards the monolayer saturation for different components. The monolayer capacity of $CO_2$ was higher than that of $CH_4$, which was in turn higher than that of $N_2$. The extended multisite Langmuir's adsorption was used to correlate the experimental absolute amounts adsorbed for each gas collectively in terms of temperature and pressure.

The kinetics of adsorption of $CO_2$, $CH_4$ and $N_2$ onto RF-ACX showed that the overall mass transfer coefficient for the adsorption of each gas increased when increasing temperature and decreased when increasing pressure. Nonetheless, the effect of pressure diminishes at high pressures for all gases. It is noteworthy that the mass transfer coefficient for various species showed different orders depending on pressures. Namely, he adsorption affinity of RF-ACX at low pressure follows the order $CH_4 > N_2 > CO_2$, whereas at high pressure the order changes to $N_2 \geq CO_2 > CH_4$. This gives a promise for RF-ACX to provide flexible selectivity variations for adsorption processes when varying the corresponding conditions.

When a clean surface of RF-ACX is concerned, the adsorption of $CH_4$ showed the highest isosteric heat of adsorption ($\sim$ 35 kJ/mol) among the three gases. The corresponding heats of adsorption for $N_2$ and $CO_2$ on a relatively clean RF-ACX surface were at $\sim$20 and $\sim$13 kJ/mol, respectively. The isosteric heats of adsorption of $CH_4$ and $N_2$ decreased with the increasing surface coverage, whereas that of $CO_2$ increased with increasing surface coverage. At high surface coverage, the isosteric heats of $CH_4$ and $CO_2$ become almost equal at $\sim$30 kJ/mol, whereas that of $N_2$ reaches $\sim$8 kJ/mol. These variable magnitudes of isosteric heats are indicative of the relative variation of the adsorption affinity of each component onto RF-ACX. Conclusively, it was shown that RF-ACX can be used effectively for separating gas mixtures containing $CO_2$, $CH_4$ and $N_2$ with variable selectivities at various conditions.

Predicted binary adsorption equilibria of the corresponding binary combinations ($CO_2$ with $CH_4$, $CH_4$ with $N_2$ and $CO_2$ in $N_2$) were analyzed and they also mostly indicated preferable adsorption of $CO_2$ from either $CH_4$ or $N_2$, and preferable adsorption of $CH_4$ from $N_2$. Furthermore, their dependence on temperature and pressure where investigated. It was shown that at certain conditions, adsorption azeotropes may be exhibited beyond which the adsorbent's selectivity is reversed.

**Acknowledgments** This publication was made possible by the support of an NPRP grant from the QNRF. The statements made herein are solely the responsibility of the authors.

## References

Al-Muhtaseb, S.A., Ritter, J.A.: Preparation and properties of resorcinol–formaldehyde organic and carbon gel. Adv. Mater. **15**, 101–114 (2003)

Al-Muhtaseb, S.A., Ritter, J.A.: Roles of surface heterogeneity and lateral interactions on the isosteric heat of adsorption and adsorbed phase heat capacity. J. Phys. Chem. B. **103**, 467–2479 (1999)

Awadallah-F, A., ElKhatat, A.M., Al-Muhtaseb, S.A.: Impact of synthesis conditions on meso- and macropore structures of resorcinol–formaldehyde xerogels. J. Mater. Sci. **46**, 7760–7769 (2011)

Czakkel, O., Székely, E., Koczka, B., Geissler, E., László, K.: Drying of resorcinol–formaldehyde gels with $CO_2$ medium. Microporous Mesoporous Mater. **148**, 34–42 (2012)

ElKhatat, A.M., Al-Muhtaseb, S.A.: Advances in tailoring resorcinol–formaldehyde organic and carbon gels. Adv. Mater. **23**, 2887–2903 (2011)

Gallegos-Suarez, E., Pérez-Cadenas, A.F., Maldonado-Hódar, F., Carrasco-Marín, F.: On the micro- and mesoporosity of carbon aerogels and xerogels. The role of the drying conditions during the synthesis processes. Chem. Eng. J. **181–182**, 851–855 (2012)

Liu, Z., Grande, A.C., Li, P., Yu, J., Rodrigues, A.E.: Multi-bed vacuum pressure swing adsorption for carbon dioxide capture from flue gas. Sep. Purif. Technol. **81**, 307–317 (2011)

Long, E., Zhang, X., Li, Y., Liu, Z., Wang, Y., Gong, M., Chen, Y.: Effect of cobalt oxide on performance of Pd catalysts for lean-burn natural gas vehicles in the presence and absence of water vapor. J. Nat. Gas Chem. **19**, 134–138 (2010)

Muleja, A.A., Mbianda, X.Y., Krause, R.W., Pillay, K.: Synthesis, characterization and thermal decomposition behaviour of triphenylphosphine-linked multiwalled carbon nanotubes. Carbon **50**, 2741–2751 (2012)

Rahman, K.A., Saha, B.B., Ng, K.C.: On thermodynamics of methane + carbonaceous materials adsorption. Int. J. Heat Mass Transfer. **55**, 565–573 (2012)

Rasines, G., Lavela, P., Macías, C., Haro, M., Ania, C.O., Tirado, J.L.: Electrochemical response of carbon aerogel electrodes in saline water. J. Electroanal. Chem. **671**, 92–96 (2012)

Ritter, J.A., Bhadra, S.J., Ebner, A.D.: On the use of the dual-process Langmuir model for unary equilibria and predicting mixed-gas adsorption equilibria. Langmuir **27**, 4700–4712 (2011)

Morales-Torres, S., Maldonado-Hódar, F., Pérez-Cadenas, A.F., Carrasco-Marín, F.: Structural characterization of carbon xerogels: from film to monolith. Microporous Mesoporous Mater. **153**, 24–29 (2012)

Tagliabue, M., Rizzo, C., Onorati, N.B., Gambarotta, E.F., Carati, A., Bazzano, F.: Regenerability of zeolites as adsorbents for natural gas sweetening: a case-study. Fuel **93**, 238–244 (2012)

Washington Policy and Analysis Inc.: Fueling the Future: Natural Gas and New Technologies for a Cleaner 21st Century, Technical Report, Washington, DC (2000). http://www.gasfoundation.org/ResearchStudies/5FTFCompleteStudy.pdf. Accessed June 2012

Xia, K., Gao, Q., Wu, C., Song, S., Ruan, M.: Activation, characterization and hydrogen storage properties of the mesoporous carbon CMK-3. Carbon **45**, 1989–1996 (2007)

Yang, R.T.: Adsorbents: Fundamentals and Applications. Wiley, Hoboken (2003)

Zhang, X., Long, E., Li, Y., Guo, J., Zhang, L., Wang, M.G.M., Chen, Y.: $CeO_2$–$ZrO_2$–$La_2O_3$–$Al_2O_3$ composite oxide and its supported palladium catalyst for the treatment of exhaust of natural gas engined vehicles. J. Nat. Gas Chem. **18**, 139–144 (2009)